ce/papers Proceedings in civil engineering

Ernst & Sohn A Wiley Brand

ORIGINAL ARTICLE

Effects of Deposition Rate on Local Stability of Wire Arc Additively Manufactured Outstand Elements

Siân Evans[1] | Nicolas Hadjipantelis[2] | Jie Wang[1]

Correspondence

Siân Evans
Department of Architecture and Civil Engineering
University of Bath
Claverton Down
BA2 7AY
Email: sie22@bath.ac.uk

[1] Department of Architecture and Civil Engineering, University of Bath, Bath, UK

[2] Department of Civil and Environmental Engineering, University of Cyprus, 1 Panepistimiou Avenue, 2109 Nicosia, Cyprus

Abstract

A great focus is currently being placed on the development of applications of Wire Arc Additive Manufacturing (WAAM) in structural engineering. To facilitate this development, an experimental programme investigating the effects of the deposition rate on WAAM 316LSi stainless steel outstand elements has been conducted. Equal angle section (EAS) stub columns with four different cross-sectional slendernesses were produced using WAAM. For each slenderness, four different deposition rates were employed; hence, overall, sixteen EAS stub columns were produced, 3D scanned and tested to examine their local stability. To keep the heat input constant between all cases, for each deposition rate, the travel speed was varied accordingly. Alongside the EAS specimens, tensile coupon testing was conducted to determine the material properties corresponding to each deposition rate. The tensile coupons were extracted at three different orientations (0°, 45° and 90°) relative to the deposition direction in order to investigate the degree of material anisotropy. In the present paper, following the description of the EAS stub column test results, the applicability of current Eurocode design rules and the Continuous Strength Method for the prediction of their design strength is assessed.

Keywords

Anisotropy, Deposition Rate, Heat input, Local Buckling, Material Properties, Stainless Steel, Stub Column Testing, Wire Arc Additive Manufacturing

1 Introduction

Wire Arc Additive Manufacturing (WAAM) is drawing attention from the construction industry due to its capability to produce large-scale freeform metallic structures [1]. To achieve high productivity, rapid deposition rates are desired. While several studies have investigated the effects of the heat input involved in WAAM on the material properties and bead geometry [2-6], the effects of the deposition rate remain unexplored. Hence, an experimental programme has been conducted to investigate the effects of the deposition rate on the material properties and local stability of WAAM stainless steel outstand elements. Four different deposition rates, under constant heat input, were investigated. The production process and the results from the tensile coupon and stub column tests are presented herein. Comparisons with existing design rules are also made.

2 Calibration of printing parameters

The WAAM production was conducted using the WAAM facility of the Steel Structures Group of the Department of Civil and Environmental Engineering of the University of Cyprus. Initial trials showed that a combination of 9 m/min wire feed speed (WFS) and 14.4 mm/s travel speed (TS) can produce a stable bead when a feedstock of 1.0 mm diameter 316LSi stainless steel wire, pulsed welding and 98%Ar–2%CO_2 shielding gas at 16 l/min flow rate are used; hence, these were chosen as the initial printing parameters and a trial wall of 20 layers was printed. The interpass temperature of 150 °C, which is below the maximum allowable temperature (typically 250–350 °C) specified in EN 1011-2 [7], was used. A continuous printing strategy was used throughout this work; alternative strategies include point-by-point printing [11-13].

The voltage and current were read at a frequency of 5 kHz. The average instantaneous power $P_{av,i}$ was calculated using Eq. 1 [11,12], where I_i and V_i are the instantaneous current and voltage respectively, and n is the total number of datapoints. The heat input (HI) was calculated using Eq. 2 [11], where η is the thermal efficiency, taken as 0.8 for MIG welding. The resulting (from the initial printing parameters) heat input of 230 J/mm was set as the target heat input (HI_t) for all printing strategies. In this manner, the effects of the heat input were isolated, ensuring that the effects of the deposition rate were solely investigated.

https://doi.org/10.1002/cepa.2354 wileyonlinelibrary.com/journal/cepa

$$P_{\mathrm{av,i}} = \frac{1}{n}\sum_{i=1}^{n} I_{\mathrm{i}} V_{\mathrm{i}} \quad (1)$$

$$\mathrm{HI} = \eta \frac{P_{\mathrm{av,i}}}{TS} \quad (2)$$

To achieve three additional deposition rates, the WFS was varied according to Table 1. The calibration process to determine the TS that would result to the target heat input is described below. Firstly, estimated voltage V_{est} and current I_{est} values were obtained from the power source. These values were used to estimate the instantaneous power $P_{\mathrm{i,est}}$, which was used in Eq. 2 to back-calculate the TS required to achieve the target heat input $\mathrm{HI_t}$. Using the resulting parameters, a test wall of 20 layers was printed; where necessary, the printing parameters were fine tuned to achieve a stable weld. The resulting HI and $P_{\mathrm{i,av}}$ were calculated using the sensor data. A second iteration of the aforementioned process was conducted to ensure that the resulting HI was as close to $\mathrm{HI_t}$ as possible.

Table 1 provides the nominal layer height h_{nom}, the theoretical deposition rate DR_{th}, as given by Eq. 3, where A is the cross-sectional area of the wire feedstock and ρ is the density of the feedstock, the measured deposition rate DR_{m} (determined by dividing the mass of the largest specimen for each strategy by the time spent actively depositing material) and the percentage difference between the actual and theoretical heat inputs and deposition rates.

$$DR_{\mathrm{th}} = \mathrm{WFS} \times A \times \rho \quad (3)$$

3 Production of coupons and stub columns

For each strategy, plates for tensile coupon extraction were produced (Fig. 1). The tensile coupons were extracted using waterjet cutting, with three coupons being extracted at 45° to the deposition direction, four at 0° and three at 90° for each strategy (apart from Strategy 1 which had six coupons at 90°). The dimensions of each coupon were based on sub-sized rectangular specimens according to [13], as shown in Fig. 3. All coupons were machined to a nominal thickness of 4.1 mm, ensuring a constant cross-section along their parallel lengths. For each strategy, four stub columns with equal angle sections (EAS) of different slenderness, as defined in Table 2, were produced (Fig. 2). The EAS were cut so that their length L was twice their nominal flange width c and their ends were cut to be perpendicular to their longitudinal axis. The EAS specimens are named according to the printing strategy and their nominal flange width; e.g. S1-50 is the specimen produced using Strategy 1 with a nominal flange width of 50 mm. Balling was roughly removed from the surface of each EAS to minimise their influence on the geometry measurements, as in previous tests [14,15].

Table 1: Printing parameters used for each strategy.

Strategy	WFS (m/min)	TS (mm/s)	WFS / TS ( )	h_{nom} (mm)	HI (J/mm)	$\frac{\mathrm{HI}-\mathrm{HI_t}}{\mathrm{HI_t}}$ (%)	DR_{th} (kg/h)	DR_{m} (kg/h)	$\frac{DR_{\mathrm{m}}-DR_{\mathrm{th}}}{DR_{\mathrm{th}}}$ (%)
1	3	4.77	0.63	1.49	225	-2.08	1.10	1.07	-2.79
2	6	9.45	0.63	1.35	229	-0.46	2.20	2.12	-3.54
3	9	14.4	0.63	1.23	239	3.94	3.30	3.18	-3.55
4	12	21.8	0.55	1.16	213	-7.29	4.40	4.07	-7.45

Table 2: Geometry and EAS stub column results.

Specimen	c (mm)	L (mm)	$\bar{b}$ (mm)	t_{av} (mm)	A_{av} (mm²)	$\bar{\lambda}_{\mathrm{av}}$	$\bar{\lambda}_{\mathrm{av,min}}$	N_{u} (kN)	δ_{u} (mm)	$N_{\mathrm{u}}/N_{\mathrm{y,av}}$	$N_{\mathrm{u}}/N_{\mathrm{y,av,min}}$
S1-50	50	100.2	45.3	5.26	480	0.46	0.51	142	1.67	0.90	0.99
S1-60	60	120.3	55.2	5.39	591	0.54	0.60	171	2.11	0.88	0.97
S1-70	70	140.2	64.6	5.35	690	0.64	0.70	195	1.63	0.86	0.95
S1-80	80	160.0	75.3	5.27	787	0.76	0.83	225	1.53	0.87	0.95
S2-50	50	100.2	45.3	5.81	528	0.33	0.37	177	1.51	1.05	1.16
S2-60	60	120.2	55.6	5.81	661	0.41	0.44	206	1.72	0.98	1.06
S2-70	70	140.5	65.4	5.84	780	0.48	0.52	241	1.41	0.97	1.05
S2-80	80	160.0	75.7	5.77	882	0.56	0.61	278	1.24	0.99	1.08
S3-50	50	100.2	46.3	6.31	598	0.38	0.41	212	1.69	1.09	1.18
S3-60	60	120.2	56.0	6.45	736	0.45	0.48	249	1.57	1.04	1.12
S3-70	70	140.2	65.9	6.16	835	0.55	0.59	273	1.27	1.01	1.09
S3-80	80	160.1	75.8	6.12	955	0.64	0.69	316	1.19	1.02	1.10
S4-50	50	100.3	46.0	5.89	553	0.40	0.45	214	1.63	1.23	1.37
S4-60	60	120.3	56.1	6.05	680	0.48	0.52	225	1.69	1.05	1.15
S4-70	70	140.3	66.0	6.03	822	0.56	0.61	271	1.24	1.04	1.14
S4-80	80	160.0	76.1	5.81	914	0.67	0.74	278	1.24	0.96	1.05

Figure 1: Printed 'ovals' for tensile coupon extraction.

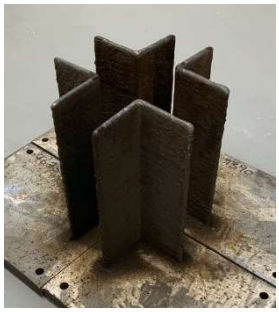

Figure 2: Printed EAS.

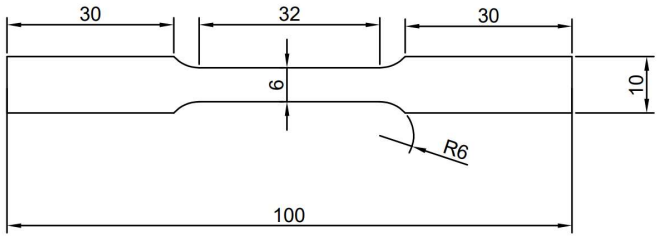

Figure 3: Tensile coupon dimensions (in mm) [10].

4 Tensile coupon test results

The tensile testing was conducted at the Department of Architecture and Civil Engineering at the University of Bath. Following the same procedure as in [14,15], the coupons were tested at room temperature using displacement control (such that the estimated strain rates over the parallel length met the requirements in EN ISO 6892-1 [16]) on an Instron 3369 50 kN testing frame. The displacement rate was changed when it was clear that the stress-strain graph had started to curve, ensuring a strain rate ≤0.00007 s^{-1} in the elastic range and ≤0.00024 s^{-1} in the plastic range. The load was measured using the load cell of the testing frame, while the strain was measured by a combination of strain gauges (in the elastic stage) and an 8 mm clip gauge extensometer (in the plastic stage).

Material anisotropy has been observed, as found by other researchers investigating WAAM stainless steel [17,18]. A typical case is shown in Fig. 4, where it is clear that the Young's Modulus varies for the different angles of extraction.

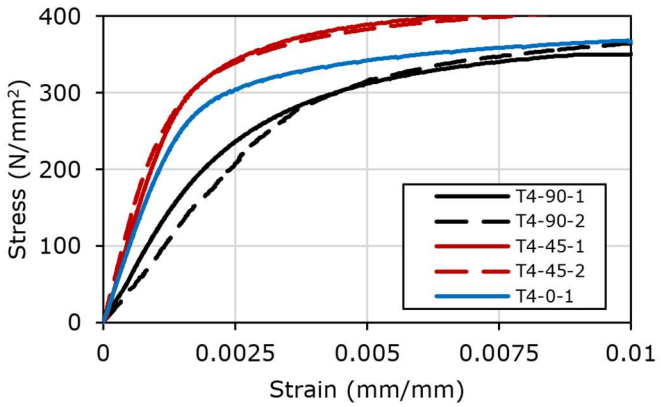

Figure 4: Initial region of the stress-strain curves for the Strategy 4 tensile coupons.

Owing to the fact that the EAS in this study were printed such that their longitudinal axes are aligned at 90° degrees to the deposition direction, the average properties from the coupons extracted at this angle are of most interest. Therefore, the average Young's Modulus E and the average 0.2% proof stress $f_{0.2}$ for coupons extracted at 90° are given for each strategy in Table 3. It is observed that for this angle of extraction, Strategies 1, 3 and 4 have similar average E, whilst Strategy 2 produces an E approximately 50% greater than the remaining strategies. In all cases, E was found to be less than the benchmark average for 316LSi stainless steel (200 kN/mm^2 [19]), but similar to values previously reported for WAAM 316LSi specimens [20]. The results for coupons extracted at the other orientations will be presented in future publications.

Table 3: Average material properties for coupons extracted at 90° to the deposition direction.

Strategy	E (kN/mm2)	$f_{0.2}$ (N/mm2)
1	99	328
2	150	319
3	104	325
4	102	316

5 Geometric measurements

The initial surface geometry of the stub columns was scanned using a Hexagon CMS 108AP 3D laser line scanner and the obtained data was analysed in MATLAB [21]. The analysis revealed that the deposition rate affects the average thickness t_{av} of the printed component, as shown in Fig. 5. This relationship is not linear, as found in literature [6]. The average of the minimum thicknesses $t_{av,min}$, which were determined as the distances between the troughs at each layer, was also determined; t_{av} and $t_{av,min}$ were used to determine the average cross-sectional area A_{av} and the average minimum cross-sectional area ($A_{av,min}$) of each EAS, as listed in Table 2, respectively. Similarly, the two slendernesses $\bar{\lambda}_{av}$ and $\bar{\lambda}_{av,min}$ were calculated using Eq. 4 [22] and t_{av} and $t_{av,min}$ for t, respectively. In Eq. 4, the average centreline width $\bar{b}$ was determined using the scan data, while $\varepsilon = [(235/f_{0.2})(E/210000)]^{0.5}$ was calculated using the average $f_{0.2}$ and E of the machined 90° tensile coupons; the buckling coefficient k_σ was taken as 1.3 based on the clamped support conditions (at the loaded edges) and pinned-free boundary conditions (along the unloaded edges) used in the tests.

$$\bar{\lambda}_p = \frac{\bar{b}/t}{28.4\varepsilon\sqrt{k_\sigma}} \quad (4)$$

6 Stub column test and results

The stub column testing was conducted at the Department of Architecture and Civil Engineering at the University of Bath. The stub columns were tested using the same method as in [13], with 9 mm thick end plates used to provide fixed end conditions. The displacements were measured using four vertical linear variable displacement transducers (LVDTs) and two horizontal ones (located in the approximate centre of each flange) as shown in Fig. 6. The specimens were tested with displacement rates between 0.15 and 0.45 mm/min, corresponding to the utilised rates before and after the ultimate load N_u,

respectively. N_u and the end-shortening at the ultimate point δ_u achieved by each specimen are given in Table 2; the ultimate loads are also given in a normalised form i.e. $N_u/N_{y,av}$ and $N_u/N_{y,av,min}$, where $N_{y,av}$ and $N_{y,av,min}$ are the squash loads, as calculated by multiplying the average yield strength of the 90° coupons with A_{av} and $A_{av,min}$, respectively.

A comparison between the normalised load (i.e. the average axial stress) versus the normalised end-shortening (i.e. vertical displacement δ divided by the initial length L) curves of specimens with the same nominal geometry but produced with different strategies is made in Fig. 7. The Strategy 1 specimen has the lowest ultimate stress. This pattern was observed in all geometries and is attributed to the fact that Strategy 1 specimens had the smallest t_{av} and thus the lowest $\bar{\lambda}_p$. As Strategy 3 led to the greatest t_{av}, it was expected that Strategy 3 specimens would have achieved the greatest ultimate stress. While this was the case for specimens with a nominal flange width of 60 mm, as shown in Fig. 7, it was not found to be the case for all other geometries; this is attributed to the variation in the material properties between different printing strategies.

For all strategies, the sections with the smallest nominal flange width (50 mm) reached the greatest ultimate stress because they were the stockiest. There is little difference between the ultimate stress levels of the remaining specimens for each strategy, as shown in Fig. 8. While all Strategy 1 specimens failed to reach the average yield stress ($f_{0.2}$) of the 90° tensile coupons, all the Strategy 3 specimens along with S2-50, S4-50, S4-60 and S4-70 achieved this stress indicating that in these specimens local buckling did not occur.

The Continuous Strength Method (CSM) [23] was developed initially to account for the contribution of material strain hardening to the resistance of steel sections. The applicability of it to the WAAM sections is assessed herein as the majority of the stub columns presented local slenderness $\leqslant$0.68 and thus may be considered as stocky. The test results are compared with the CSM predictions in Fig. 9, where it can be seen that the test results follow closely the CSM curve when either $\bar{\lambda}_{av}$ or $\bar{\lambda}_{av,min}$ are used. The ultimate loads predicted using CSM are given in Table 4; $N_{u,1\text{-CSM}}$ and $N_{u,2\text{-CSM}}$ were calculated using A_{av} and $A_{av,min}$ respectively. As shown in Fig. 10, the use of $A_{av,min}$ provides better predictions than the use of A_{av}, with the average $N_u/N_{u,1\text{-CSM}}$ being 0.92 compared to 1.03 for $N_u/N_{u,2\text{-CSM}}$.

In contrast, using the Eurocode's Effective Width Equation [21] to predict N_u gives an average $N_u/N_{u,1\text{-EC3}}$ of 1.01 and $N_u/N_{u,2\text{-EC3}}$ of 1.11, where $N_{u,1\text{-EC3}}$ and $N_{u,2\text{-EC3}}$ are based on A_{av} and $A_{av,min}$ respectively. While $N_{u,1\text{-EC3}}$ gives a closer average prediction than $N_{u,2\text{-CSM}}$, the data is slightly more spread out (with standard deviations for $N_{u,1\text{-EC3}}$ and $N_{u,2\text{-CSM}}$ being 0.087 and 0.086 respectively), as shown in Fig. 11.

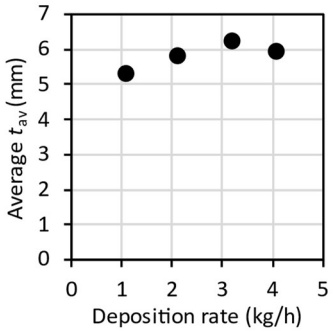

Figure 5: The average t_{av} for each strategy.

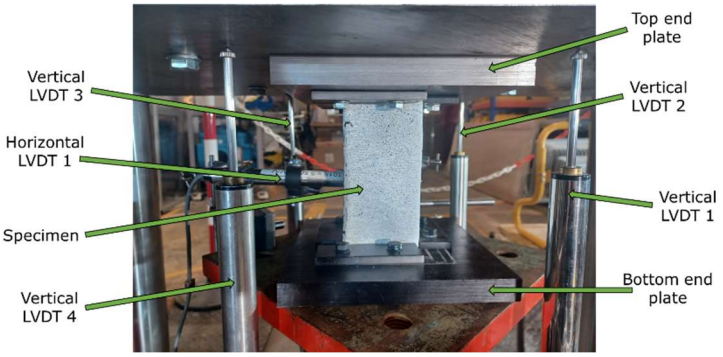

Figure 6: The setup of the stub column tests (with horizontal LVDT 2 being hidden behind the front-facing flange).

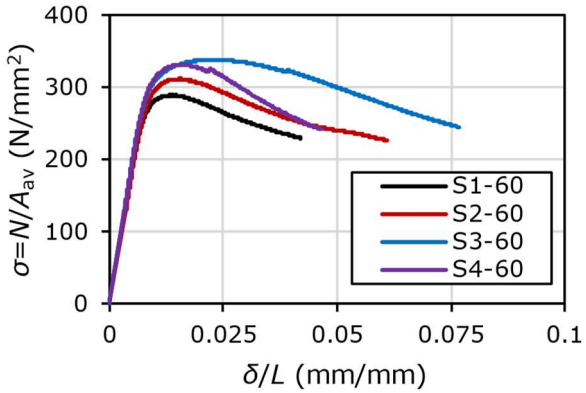

Figure 7: Normalised load vs end-shortening curves for samples with a nominal flange width of 60 mm.

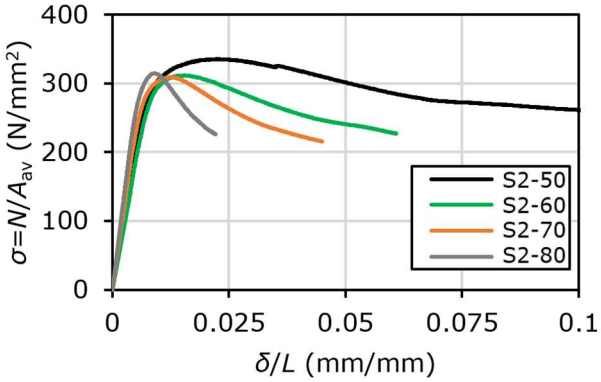

Figure 8: Normalised load vs end-shortening curves for samples produced using Strategy 2.

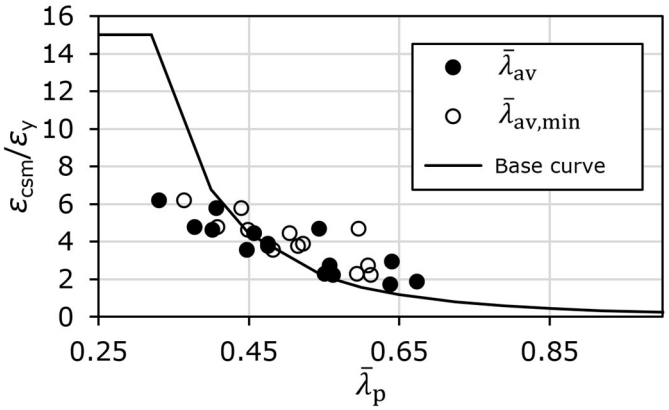

Figure 9: Comparison of the test results with the CSM predictions.

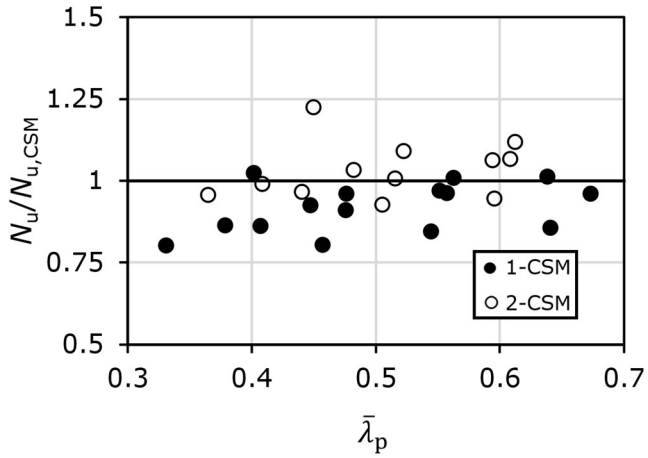

Figure 10: Comparison of N_u to $N_{u,1\text{-CSM}}$ and $N_{u,2\text{-CSM}}$.

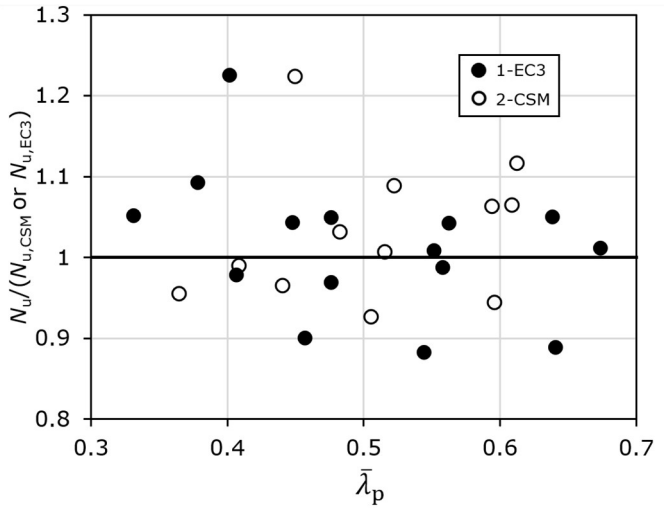

Figure 11: Comparison of Nu to $N_{u,2\text{-CSM}}$ and $N_{u,1\text{-EC3}}$.

Table 4: Predicted ultimate loads using the Continuous Strength Method [23].

Specimen	N_u (kN)	$N_{u,1\text{-CSM}}$ (kN)	$N_{u,2\text{-CSM}}$ (kN)	$N_u/N_{u,1\text{-CSM}}$	$N_u/N_{u,2\text{-CSM}}$
S1-50	142	176	153	0.803	0.927
S1-60	171	203	181	0.843	0.944
S1-70	195	228		0.855	
S2-50	177	221	186	0.802	0.955
S2-60	206	239	213	0.861	0.965
S2-70	241	265	239	0.909	1.007
S2-80	278	289	261	0.962	1.065
S3-50	212	246	215	0.864	0.989
S3-60	249	270	242	0.924	1.032
S3-70	273	282	257	0.969	1.062
S3-80	316	313		1.012	
S4-50	214	210	175	1.022	1.224
S4-60	225	235	207	0.96	1.089
S4-70	271	269	243	1.008	1.117
S4-80	278	289		0.96	
			Mean	0.92	1.03
			Standard deviation	0.07	0.09

7 Conclusions

The results of an experimental programme which investigated the effects of the deposition rate on the material response and local buckling behaviour of WAAM stainless steel outstand elements have been presented herein.

Tensile coupon tests and stub column tests on equal angle WAAM sections were conducted. The specimens were produced using four different deposition rates while maintaining constant heat input. To achieve this, an iterative process, which involved the determination of the average instantaneous power utilised in the WAAM process, was used.

The tensile coupon tests revealed significant anisotropy in the material properties of the 316LSi stainless steel used for the purposes of this study. The influence of the deposition rate on the geometric properties and the local stability of the equal angle sections has been determined. The results from the stub column tests have been presented and comparisons have been made with the design provisions of Eurocode 3 and of the Continuous Strength Method.

Further work will include the analysis of the data obtained using Digital Image Correlation with the aim to obtain further insights on the development of the surface strain fields during the stub column tests; tensile tests on as-built specimens will also be conducted to determine the effective properties of the studied WAAM elements.

References

[1] Gardner, L. (2022) *Metal additive manufacturing in structural engineering – review, advances, opportunities and outlook. Structures.* Vol. 47, 2178-2193.

[2] Yildiz, A. S. et al. (2020) *Wire arc additive manufacturing of high-strength low alloy steels: study of process parameters and their influence on the bead geometry and mechanical characteristics. Int J of Adv Manuf Technol*. Vol 108, no 11, 3391-3404.

[3] Aldalur, E. et al. (2020) *High deposition wire arc additive manufacturing of mild steel: strategies and heat input effect on microstructure and mechanical properties, J of Manuf Process*. Vol 58, 615-626.

[4] Chen, C. et al. (2023) *Effect of equivalent heat input on WAAM Al-Si Alloy. Int J of Mech Sci.* Vol 238.

[5] Fang, Q. et al. (2023) *Effect of heat input on microstructural and mechanical properties of high strength low alloy steel block parts fabricated by wire arc additive manufacturing. Materials Today Comm.* Vol 34.

[6] Dinovitzer, M. et al. (2019) *Effect of wire and arc additive manufacturing (WAAM) process parameters on bead geometry and microstructure. Add Manuf* Vol 26, 138-146.

[7] BS EN 1011-2:2001 *Welding – recommendations for welding of metallic materials – Part 2: arc welding of ferritic steels.*

[8] Laghi, V. et al. (2021) *Experimental behaviour of Wire-and-Arc Additively Manufactured stainless steel rods*. Eurosteel, Sheffield, UK, September 2021.

[9] Silvestru, V. et al. (2021) *Performance under tensile loading of point-by-point wire and arc additively manufactured steel bars for structural components. Materials and Design.* Vol 205, 109740.

[10] Silvestru, V. et al. (2023) *Structural behaviour of point-by-point wire arc additively manufactured steel bars under compressive loading. J of Construct Steel Research.* Vol. 207, 107982.

[11] Quintino, L. et al. (2013) *Heat input in full penetration welds in gas metal arc welding (GMAW). Int J Adv Manuf Technol.* Vol 68, no. 9-12, 2833-2840.

[12] Joseph, A. et al. (2003) *Measurement and calculation of arc power and heat transfer efficiency in pulsed gas metal arc welding. Sci and Technol of Welding & Joining*. Vol 8, 400-406.

[13] ASTM E8/E8M-13 (2013) *Standard Test Methods for Tension Testing of Metallic Materials.*

[14] Evans, S.; Wang, J. (2022) *Material Properties and Local Stability of WAAM Stainless Steel Plates with Different Deposition Rates.* ICASS, Chengdu, China, May 2022.

[15] Evans, S. et al. (2023) *Material Properties and Local Stability of WAAM Stainless Steel Equal Angle Sections. Engineering Str*.

[16] BS EN ISO 6892-1:2019 *Metallic materials, tensile testing, method of test at room temperature*.

[17] Kyvelou, P. et al. (2020) *Mechanical and microstructural testing of wire and arc additively manufactured sheet material. Materials and Design.* Vol 192.

[18] Hadjipantelis, N. et al. (2022) *Description of anisotropic material response of wire and arc additively manufactured thin-walled stainless steel elements. Thin-Wall Str.* Vol 171.

[19] BS EN 10088-2: 2014 *Stainless Steels Part 2: Technical delivery conditions for sheet/plate and strip of corrosion resisting steels for general purposes*.

[20] Cunningham, C. et al. (2019) *Characterisation of Austenitic 316LSi Stainless Steel Produced by Wire Arc Additively Manufacturing with Interlayer Cooling.* Int Solid Freeform Fabrication Symposium, Austin, USA, 2019.

[21] MATLAB, 2019.

[22] European Committee for Standardization (CEN) Eurocode 3: Design of steel structures. Part 1-4: *General rules – Supplementary rules for stainless steels*. EN 1993-1-4 (2006).

[23] Afshan, S.; Gardner, L. (2013) *The Continuous Strength Method for Structural Stainless Steel Design. Thin-walled Str.* Vol 68, 42-49.